scientific reports

OPEN

Facile synthesis of anthranilic acid based dual functionalized novel hyper cross-linked polymer for promising CO_2 capture and efficient Cr^{3+} adsorption

Amin Abid[1,6], Saqlain Raza[1,6], Ahmad Kaleem Qureshi[1✉], Sajjad Ali[2], Isham Areej[1,6], Shahid Nazeer[1], Bien Tan[3], Wedad A. Al-onazi[4], Muhammad Rizwan[5✉] & Rashid Iqbal[2]

A novel hyper cross-linked polymer of 2-Aminobenzoic acid (HCP-AA) is synthesized for the adsorption of Cr^{3+} and CO_2. The Brunauer–Emmett–Teller surface area of HCP-AA is 615 m^2 g^{-1}. HCP-AA of particle size 0.5 nm showed maximum adsorption of Cr^{3+} for lab prepared wastewater (93%) while it was 88% for real industrial wastewater. It is might be due to electrostatic interactions, cation-π interactions, lone pair interactions and cation exchange at pH 7; contact time of 8 min; adsorbent dose 0.8 g. The adsorption capacity was calculated 52.63 mg g^{-1} for chromium metal ions at optimum conditions. Freundlich isotherm studies R^2 = 0.9273 value is the best fit and follows pseudo second order kinetic model (R^2 = 0.979). The adsorption is found non-spontaneous and exothermic through thermodynamic calculations like Gibbs free energy (ΔG), enthalpy change (ΔH) and entropy change (ΔS) were 6.58 kJ mol^{-1}, – 60.91 kJ mol^{-1} and – 45.79 kJ mol^{-1} K^{-1}, respectively. The CO_2 adsorption capacity of HCP-AA is 1.39 mmol/g with quantity of 31.1 cm^3/g (6.1 wt%) at 273K while at 298 K adsorption capacity is 1.12 mmol/g with quantity 25.2 cm^3/g (5 wt%). Overall, study suggests that carboxyl (–COOH) and amino (–NH$_2$) groups may be actively enhancing the adsorption capacity of HCP-AA for Cr^{3+} and CO_2.

Keywords Polymers, Adsorption, Heavy metals, Carbon dioxide, Chromium

There is no life without clean drinking water and fresh air but due to industrialization and population bloom, clean sources of water are declining day by day and fresh air is polluted with primary and secondary air pollutants[1–3]. Despite its huge abundance everywhere, clean water is very limited as compared to its use[4,5]. Heavy metals have serious toxic effects and cause serious diseases like[6] diarrhea, cardiovascular diseases, genotoxicity, lung diseases, cancer, damage to kidneys and bones, anemia, and eczema of skin etc[7–10].

Porous polymers are now a days, extensively used because they have important scientific and day-today applications such as heavy metal uptake, gas adsorption, drug delivery system, photo catalysis, super capacitors and renewable energy sources due to their novel features such as high BET surface area, microporous structure, high thermal stability and availability of a variety of functional groups[11–13]. The porous polymers can be classified as macroporous having pores larger than 50 nm, mesoporous having pores between 2 and 50 nm and microporous having pores smaller than 2 nm. The hyper cross-linked polymer is a type of pure organic materials and it exhibits highly cross-linked morphology. The HCP was first developed by Davankov and Tsyrupa in 1970s[14]. They synthesized HCP of polystyrene by using post crosslinking of the linear polystyrene chains from Friedel Craft reaction[15–17]. The HCPs synthesis starts from several aromatic monomers such as benzene and derivatives of benzene[18]. The first HCP was based on linear polystyrene (HCL-PS) precursor[19–21].

[1]Department of Chemistry, University of Sahiwal, Sahiwal 57000, Pakistan. [2]Faculty of Agriculture and Environment, The Islamia University of Bahawalpur, Bahawalpur 63100, Pakistan. [3]Huazhong University of Science and Technology (HUST), Wuhan, China. [4]Department of Chemistry, College of Science, King Saud University, P.O. 22452, 11495 Riyadh, Saudi Arabia. [5]Institute of Crops Science and Resource Conservation (INRES), University of Bonn, Bonn, Germany. [6]These authors contributed equally: Amin Abid, Saqlain Raza and Isham Areej. ✉email: akq999@yahoo.com; m.rizwan@uni-bonn.de

1

Now a day, adsorption is considered as one of the most efficient method for removal of heavy metals[18,22,23]. Hybrid porous materials such as HCPs are extensively applied as adsorbents because of their large pore volume, greater surface area, strong chemical and thermal stabilities, low cost and easy synthesis[24,25]. The efficiency of these adsorbents is measured by different factors such as stability, typical adsorption parameters as well as functional sites providing specific adsorbate and adsorbent interactions like hydrogen bonds, π–π interactions and electrostatic interactions etc. Due to these interactions, different polymers are used in field of medicine as drug delivery, catalysis[26], and adsorption[27,28].

Tan and co-workers presented a cost-effective technique towards the production of micro-porous polymers of different types by using aromatic building blocks[29,30] for different applications such as, heterogeneous catalysis, semiconductors, luminescence, water treatment and gas storage etc. The highly porous polymer was synthesized by Friedel–Craft alkylation with self-condensation benzyl alcohol aromatic mono-hydroxyl-methyl compounds[29,31,32]. In past, activated carbon and zeolite were also used for adsorption and removal of metal ions but they showed low adsorption ability[19,33–39].

James et al. synthesized HCP based on derivatives of sulphonated materials in which 4,4bischloromethyl 1,1 biphenyl was used as sulphonated material. New HCPs were synthesized and named as SHCP 1 and SHCP 2. The SHCP 1 was synthesized by metal free alkylation reaction. While, SHCP 2 was synthesized by Friedel Crafts reaction catalyzed by Lewis's acid. These two polymers have large surface area of 500 m^2 g^{-1}. SHCP 1 showed excellent adsorption properties for ions of Sr and Cs in an aqueous solution. A maximum uptake was 95.6 mg g^{-1} for Sr and 273 mg g^{-1} for Cs. These polymers were also shows good adsorption properties for the adsorption of Na, K, Mg and Ca and follow the pseudo second order reactions[21,40]. A HCP of iminodiacetic acid (IDA-HCP) for water purification from heavy metals ions is prepared. The synthesized polymer exhibited excellent adsorption properties because of the presence of carboxylate and amino groups. These functional groups make IDA-HCP excellent candidate for the adsorption of different metals including Zn^{+2}, Mg^{+2}, Hg^{+2} and others[41,42].

A hyper cross-linked nanometer-sized chelating agent, denoted as HCNSCR, was successfully synthesized and experimental findings unveiled that HCNSCR exhibited notable adsorption capacities for the targeted metal ions, with values of 1.2 mmol/g for Pb, 1.0 mmol/g for Cd, and 0.9 mmol/g for Zn. Furthermore, the optimal pH range for achieving the highest adsorption performance was identified to fall between 5.5 and 6.3. To describe the adsorption behavior more comprehensively, the researchers employed a Langmuir isotherm model; it has been found that it provided an adequate match to the adsorption data. In addition, a pseudo-second-order pattern was observed in the adsorption kinetics[37,38]. The analysis conducted by Podkoscielna et al. involved the modification of commercially available St DVB (styrene–divinylbenzene) resin by introducing thiol (SH) groups into the polymer. The thiol groups were incorporated into St DVB by treating it with H_2SO_4 followed by either $SnCl_2$ or $POCl_3$. The purpose of the modification was to investigate the ability of the St DVB SH material to remove heavy metal ions (Cu^{+2}, Zn^{+2}, Cd^{+2}, Pb^{+2}, and Ni^{+2}) from aqueous solutions. The results indicated that the novel modified polymer exhibited adsorption behavior in accordance with the Langmuir and Freundlich isotherm models[37,43–45].

The most confronting challenge for human is global warming. The reason behind is the rapid increase in carbon dioxide concentration in atmosphere due to anthropogenic activities[46]. The most facile way to eliminate it is carbon capture and its storage (CCS). Initiation of CCS is too expensive. In some industries and power plants, post combustion capture (PCC) technology is used due to its medium feasibility, less cost than CCS, and easy installation without major modifications. Recently, Monoethanolamine (MEA) scrubbing is set as standard for PCC technology but it has some drawbacks to power plants. It is corrosive as well as need high energy for rejuvenation[47,48].

The research and development of novel technologies and materials, that selectively capture CO_2, need growing attention because the classical method of adsorbing CO_2 using amine solution has various drawbacks, including less economical regeneration and equipment corrosion. Zeolites and activated carbon are the primary solid adsorbents for CO_2 capture. In contrast, porous materials are an alternate method of capturing CO_2 and have gained a lot of attention in recent years. The main advantages of porous materials are affordability, convenience of use, high chemical and thermal stability, and strong adsorption of CO_2[49].

Unfortunately, due to strong affinity for H_2O, MOFs, belong to porous crystalline materials; have limited use under high humidity. It is also difficult for these POPs to adsorb CO_2 more than 30% wt% at 0 °C and 1.0 bar[50]. Fortunately, a large number of alternative organic porous materials have been thoroughly investigated for CO_2 adsorption, including polymers of intrinsic micro porosity (PIMs), conjugated microporous polymers (CMPs), HCPs, and covalent organic frameworks (COFs). Porous carbons have demonstrated potential for CO_2 adsorption because of their high specific surface area, large pore volume, and adjustable surface[51,52].

The main features of a carbon dioxide adsorbent include high CO_2 selectivity, greater CO_2 adsorption capability, minimal heat of adsorption, good chemical endurance, significant thermal and mechanical durability, fabrication scalability, suitable morphology, low toxicity and cost affectivity. When choosing CO_2 adsorbents, excellent CO_2 acceptability at low pressures is a crucial factor[17]. Therefore, designing physical adsorbents with protic electronegative functions by the introduction of nitrogen groups like amine and amide is valuable fabrication with high CO_2 selectivity[47,53].

Using melamine and resorcinol, Bing et al. created a porous carbon that was doped with nitrogen. They discovered that as the nitrogen content increased, it increased the CO_2 adsorption. At the temperature of 273 K and pressure 1.0 bar, Nandi et al. reported that N-doped activated carbon monoliths achieved remarkable CO_2 adsorption of 506 mg/g[48,54]. Triazine had also been utilized as a building block in recent times to create HCPs with nitrogen in the backbone. Triazine-based HCPs are regarded as innovative materials for gas sorption research due to their exceptional CO_2 selectivity over N_2[55,56].

In this study, the fabrication of 2-Aminobenzoic Acid based dual functionalized polymer (HCP-AA) by Friedel Crafts reaction is reported by using cost effective and less toxic cross-linker CCl_4, this is the novelty of this research. Previously in literature mostly used cross-linkers were having toxicity as well as they are expensive

like formaldehyde dimethyl acetal (FDA). Furthermore, the use of same adsorbent for air purification and water treatment is also a novel concept. Industrial wastewater were used to determine the efficiency of HCP-AA and got promising results. The synthesized HCP has microporous structure, which make it excellent candidate for adsorption studies. The adsorption capacity of HCP-AA for chromium metal ions and CO_2 gas is determined. The adsorption capacity is 52.63 m g g^{-1} for chromium metal ions and 1.3 9 mmol for CO_2 at optimum conditions. Moreover, this HCP-AA can be recycled with minimum decrease in adsorption capacity. The potent adsorption capacity of HCP-AA is due to its high surface area, abundant porosity, oxygen and nitrogen rich nature. While, this synthesis has some drawbacks as it is time taking as well as requires high consumption of energy. Our research group is working to resolve these problems.

Materials and methods
Materials
Anthranilic acid (monomer), Carbon tetrachloride (cross-linker), Dichloroethane (DCE) (solvent), Ferric chloride (catalyst), Ethanol and Chromium Chloride were obtained from Sigma Organics and used as received in their pure form.

Fabrication of hyper cross-linked polymer of anthranilic acid (HCP-AA)
In a round bottom flask fitted with condenser carrying 10 mL of solvent (Dichloroethane), 0.3 g of aromatic monomer (anthranilic acid), 1 mL of cross-linker (CCl_4) and 0.3 g of Ferric Chloride ($FeCl_3$), used as a catalyst, were continuously mixed and heated in an oil bath. Initially, temperature was maintained at 45 °C for 4–5 h, and then raised to 80–85 °C for 19–20 h till product was formed. The thick paste like appearance indicates the syntheses of HCP-AA which was washed with ethanol till pure HCP-AA was obtained after the removal of excessive solvent and $FeCl_3$ (washed until brown color of $FeCl_3$ disappeared). After filtrations, purified product was collected in china dish and dried at 100 °C in an oven[57,58].

Equipment
FTIR spectra were acquired using a Thermo Nicolet Nexus 670 spectrophotometer. Elemental composition analysis of the hyper cross-linked polymers (HCPs) was conducted through Energy Dispersive X-ray Spectroscopy (EDX). Scanning Electron Microscope (SEM) imaging and analysis were performed using a Zeiss Ultra-55 instrument. Transmission Electron Microscope (TEM) analysis was conducted with a JEM-2100 plus microscope. X-ray Diffraction (XRD) powder analysis of the synthesized polymer samples was carried out using a Smart Lab TM 3 kW X-ray diffractometer. Thermogravimetric analysis was carried out by using Netzsch Jupiter thermal analyzer. To determine the BET surface area, pore volume, pore size and nitrogen adsorption/ desorption isotherms of the HCP-AA, Micro-metrics ASAP 2020 M and porosity analyzer from Micrometrics, USA were used.

Results and discussion
Characterization of HCP of anthranilic acid (HCP-AA)
Physical appearance
Appearance of HCP-AA was amorphous and black in color that is shown in Fig. 1.

Physical properties of HCP-AA
Physical properties of HCP-AA are shown in Table 1, which shows that HCP-AA melts at temperature above 400 °C.

Figure 1. Physical appearance of HCP-AA.

Sr. No	Properties	Results
1	Melting Point	400 °C
2	Physical state	Amorphous
3	Color	Black

Table 1. Physical properties of HCP-AA.

Chemical equation for synthesis of HCP-AA
Chemical equation for the preparation of anthranilic acid based hyper cross-linked polymer is shown in Fig. 2.

Mechanism of synthesis of HCP-AA
Figure 3 depicts the possible reaction mechanism for HCP-AA synthesis via Friedel Craft alkylation.

FT-IR results of HCP-AA
The FTIR spectrum of the HCP-AA is represented in Fig. 4. The peak, having medium intensity is shown at 1590 cm^{-1} that may indicates the presence of the N–H bond. The peak, having medium intensity which is observe at 1508 cm^{-1}, indicates the presence of the C=C bond stretching in benzene ring. The hydroxyl group of carboxylic acid also involved in hydrogen bonding this is indicated by the presence of weak peak at 1314 cm^{-1} the presence of C–N bond is indicated by the weak peak at 1213 cm^{-1}. Weak intensity peak at 1122 cm^{-1} indicates the presence of C–C bond of benzene ring. The most important and prominent peak at 715 cm^{-1} indicates the cross linking by C–Cl bond which may prove the synthesis of HCP-AA.

Energy dispersive X-ray spectroscopy
HCP-AA have carbon, nitrogen, oxygen and chlorine elements. The percentage of carbon was 65.84% that was the highest percentage of all other elements. Similarly, it had nitrogen of about 24.76, oxygen 7.87%, chlorine 1.32% as shown in Table 2 and Fig. 5. It also contains aurum 0.22% that might be come at the time of coating during SEM analysis.

SEM and TEM results of HCP-AA
The TEM and SEM analysis (Figs. 6 and 7) suggests that HCP-AA had porous structure and due to presence of abundant pores, it had excellent surface area. BET surface area of HCP-AA is 615 m^2 g^{-1}. Both SEM and TEM results prove that these materials are very suitable for uptake of Cr^{3+} and CO$_2$ due to their porous structure.

XRD analysis
From XRD pattern of HCP-AA (Fig. 8), we conclude that there is no sharp peak at 2θ and it has some noisy pattern, which suggests that it is amorphous in nature.

Pore size distribution
Pore size distribution of HCP-AA was examined. The results, extracted from Fig. 9, suggests that the pore width from ranges from 0.1 to 135 nm. It was measured by sorption analysis using nitrogen gas.

N$_2$ adsorption–desorption isotherms
The N$_2$ adsorption/ desorption isotherms of HCP-AA revealed the instantaneous uptake of N$_2$ gas at low pressure which suggests that abundant number of micropores are present while the gas uptake at moderate pressure is
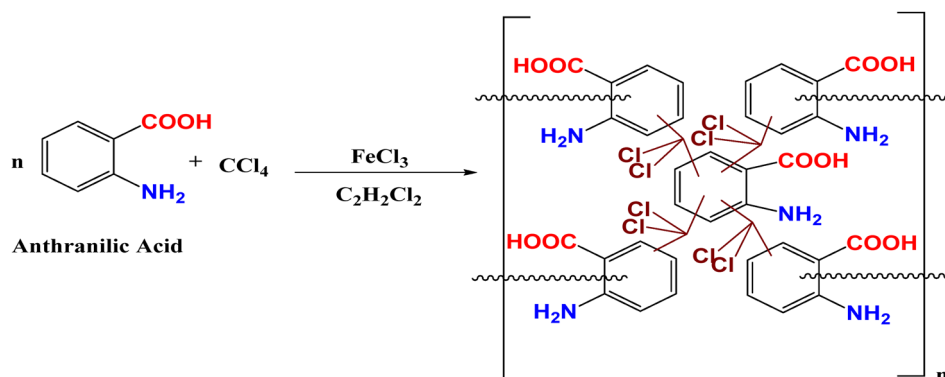

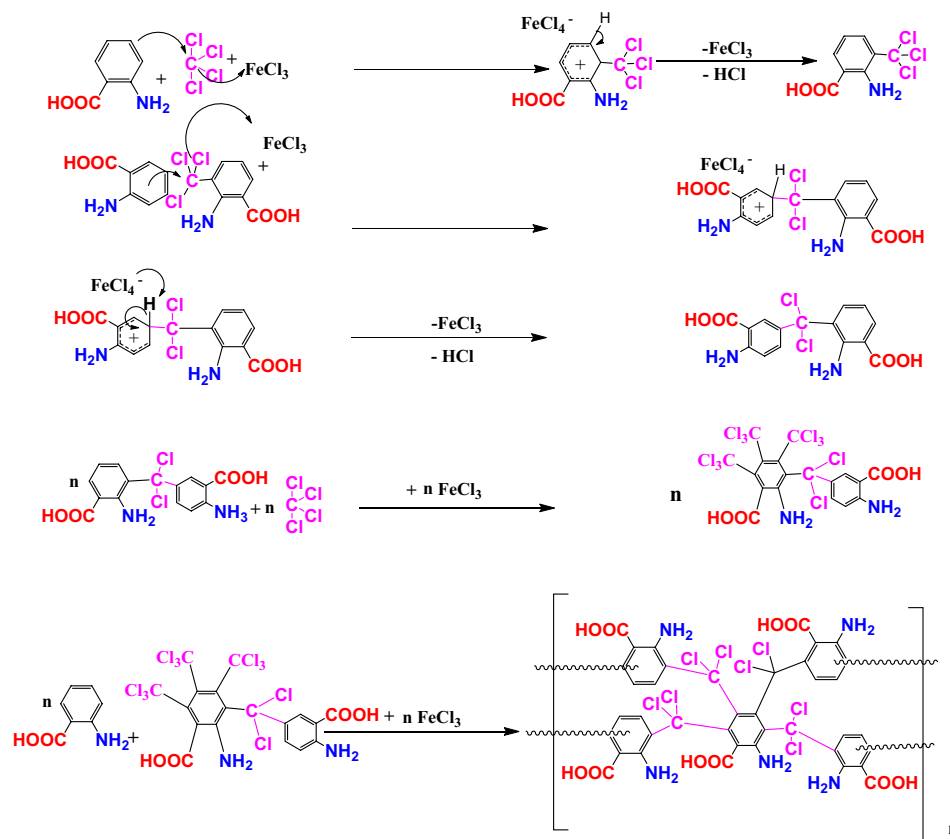**Figure 2.** Chemical equation for synthesis of HCP-AA.

4

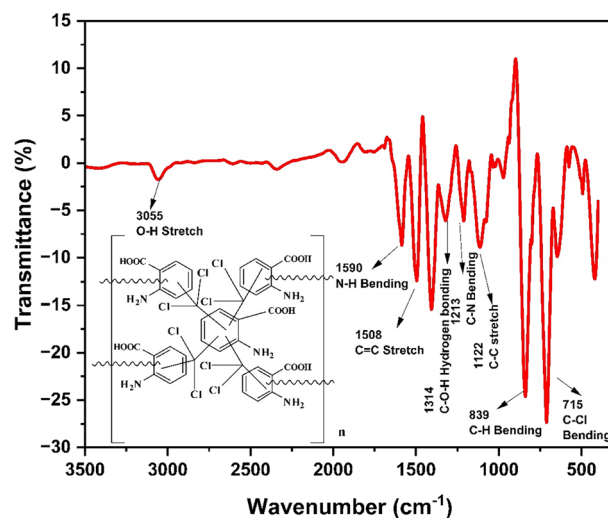**Figure 3.** Possible reaction mechanism for synthesis of HCP-AA.

Figure 4. FTIR spectra of HCP-AA.

attributed the presence of mesopores. Gas uptake at high pressure might be because of macropores as indicated in Fig. 10.

Thermogravimetric analysis
To further study the structural robustness and stability of HCP-AA, TGA was applied under inert nitrogen (N_2) gas atmosphere where temperature ranges of 20–800 °C as shown in Fig. 11. It signified that the HCP-AA was stable up to 400 °C due to highly cross-linked structure and abundance of nitrogen groups. The small mass loss under 100 °C could be the result of moisture and trapped solvent.

Element	Weight%	Atomic%	Error%
Carbon	59.36	65.84	4.92
Nitrogen	26.03	24.76	13.23
Oxygen	9.45	7.87	16.45
Chlorine	2.24	1.32	20.34
Aurum	2.76	0.22	11.06

Table 2. EDX results showing the percentage composition of HCP-AA.
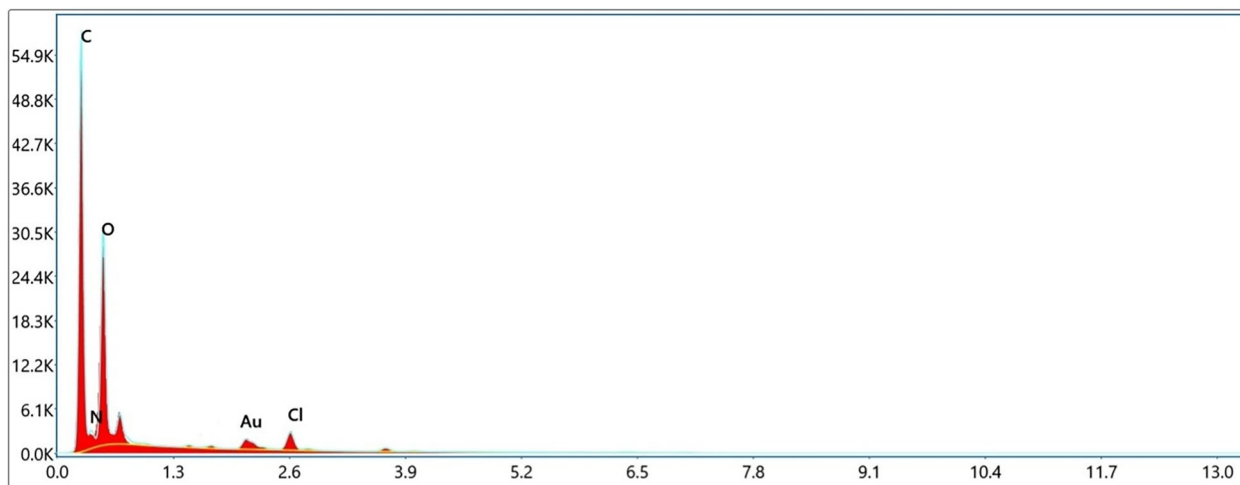
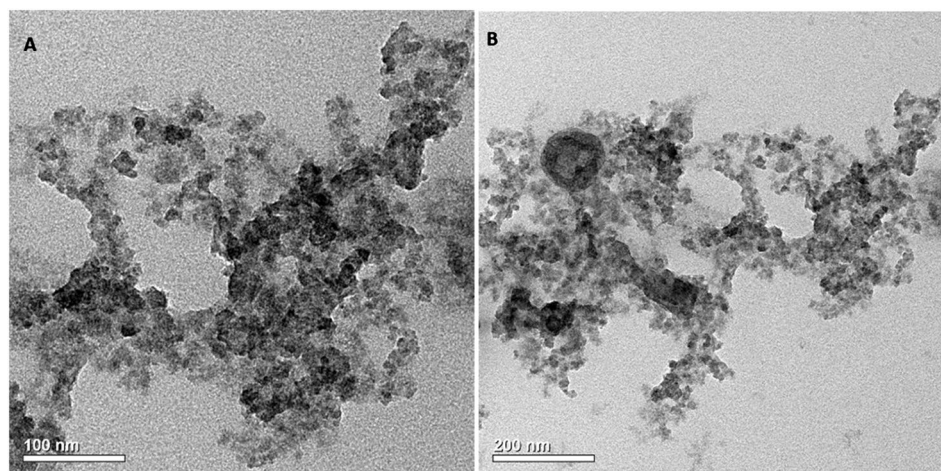**Figure 5.** EDX graph showing composition of HCP-AA.

Figure 6. TEM Images of HCP-AA.

UV–Vis spectroscopy
All hyper cross-linked polymers showed absorption in both ultraviolet and visible region. HCP-AA also absorbed light in UV and VIS region and it showed lambda max at 428 nm with absorbance 1.389, which is shown in Fig. 12.

Application of HCP-AA in removal of heavy metals
HCPs of different aromatic compounds are excellent adsorbents having remarkable properties for the uptake of an organic pollutant, dyes and the heavy metals due to their low cost, easy synthesis and greater surface area with large number of pores. A standard solution of 1000 mg L^{-1} of chromium metal was prepared by mixing 1.631 g of CrCl$_3$ to 1 L of distilled water. Standard solution of five different concentrations (10–50 mg L^{-1}) was prepared with a gap of 10 mg L^{-1}, respectively. The solutions of lower concentrations are difficult to analyze
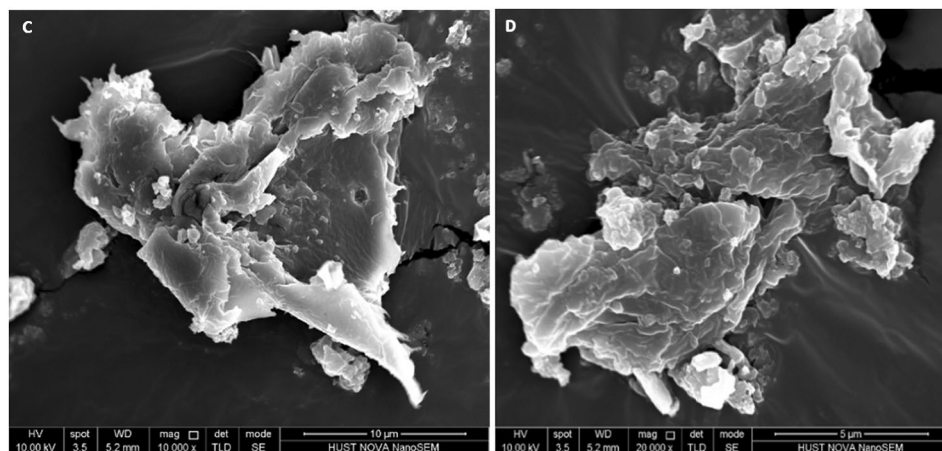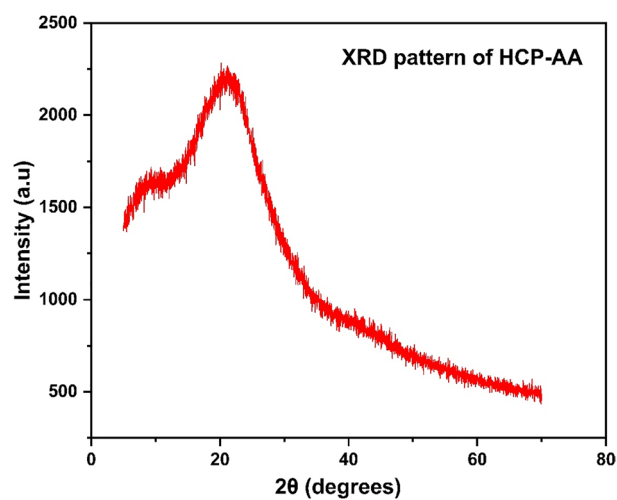
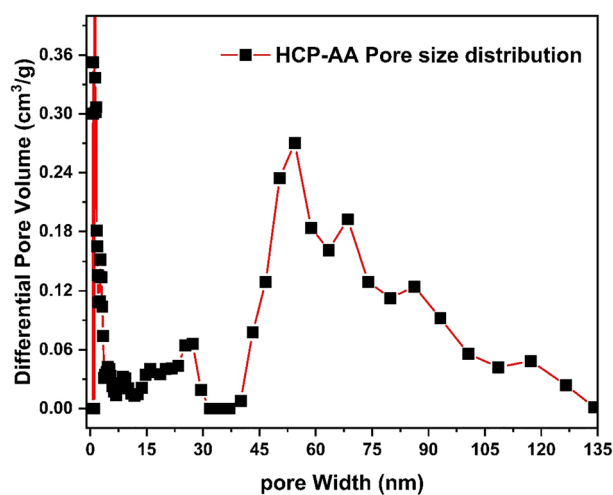**Figure 7.** SEM images of HCP-AA.

Figure 8. XRD graph of HCP-AA.

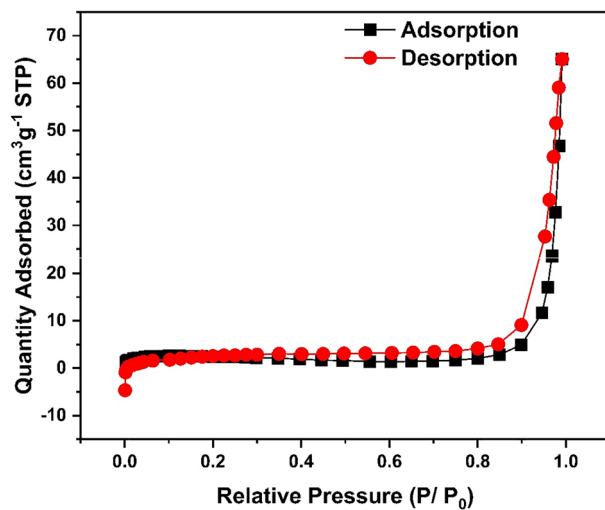**Figure 9.** Pore size distribution of HCP-AA.

Figure 10. N_2 adsorption—desorption isotherms of HCP-AA.
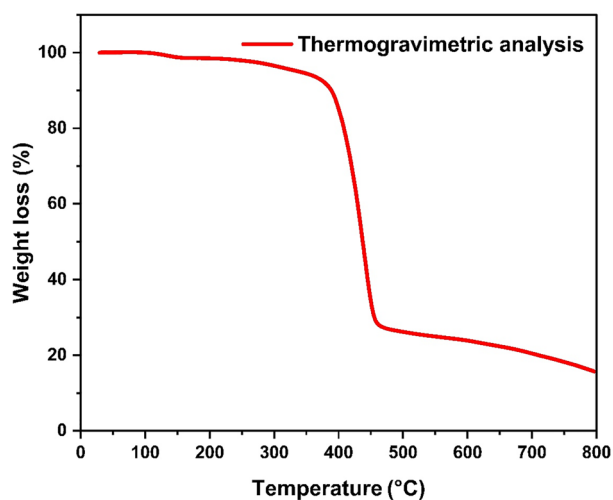

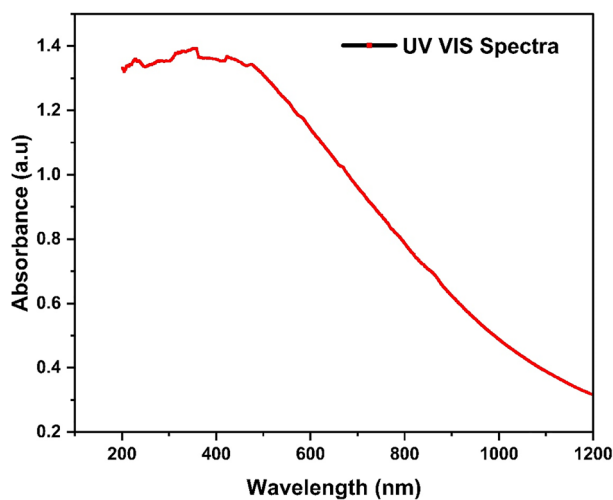**Figure 11.** Thermogravimetric analysis of HCP-AA.

Figure 12. UV–Vis graph of HCP-AA.

using AAS and the results are not reliable[59]. The synthesized HCP-AA is grinded well and thoroughly washed with ethanol followed by water until pH 7.0 was obtained. This is done to make sure the removal of all possible impurities. After this 0.8 g of purified HCP-AA was added to each prepared standard solution. These conical flasks were placed on the rotary shaker and stir at 160 rpm at 298 K for 12 min. The solution was filtered and 230ATS atomic absorption spectrophotometer (AAS) was applied to determine the concentration of Cr^{3+} from sample water. The AAS is a modern technique that is used for measurement of heavy metals in samples like the water. The percentage adsorption of HCP-AA for Cr^{3+} was 93% at optimum conditions. To perform adsorption experiment on real water sample, sample was collected from Royal leather industries Limited Lahore, Pakistan. The percentage adsorption of HCP-AA for Cr^{3+} in real wastewater sample is 88%. Decrease in percentage removal is caused by interfering ions present in real water sample. The percentage removal was calculated by using Eq. (1).

$$\text{Percentage removal of metal} = \frac{C_o - C_e}{C_o} \times 100 \qquad (1)$$

FTIR analysis of HCP-AA before and after adsorption
Figure 13 shows the FTIR spectra of HCP-AA before and after an adsorption of Cr^{3+} metal ions. The –OH group stretching peak appeared at 3055 cm^{-1} before adsorption, while after adsorption it is depressed and shifted to lower wavenumber (3045 cm^{-1}), which may indicates the chemical adsorption of Cr^{3+} metal ions by –OH group of HCP-AA. This peak is not completely disappear after adsorption that may indicates that the HCP-AA is reusable for adsorption. The other peaks such as C–Cl bending 715 cm^{-1}, C–H bending 839 cm^{-1} peaks merged, broaden and shifted to 687 cm^{-1} as chlorine may utilized its loan pair to adsorb Cr^{3+}. While C–C stretching, C–N bending and C–O–H hydrogen bonding peaks were appeared in HCP-AA at 1122 cm^{-1}, 1213 cm^{-1} and 1314 cm^{-1} respectively, these functionalities peaks also broaden, merged together and centered at 1128 cm^{-1} to justify their role in adsorption. Similarly peak 1508 cm^{-1} belonged to C=C stretching and N–H bending at 1590 cm^{-1} were depressed and broaden at position 1560 cm^{-1} to elaborate the fact that N nitrogen loan pair and pi-electronic cloud of C=C played a vital role in adsorption phenomenon. Some small sharp peaks appeared between the 450–550 cm^{-1} were merged to form a single wide peak at point 542 cm^{-1}, which may indicates Cr and O interaction after the adsorption.

Mechanism of heavy metal adsorption
Nitrogen containing materials are attractive for the heavy metal ions uptake due to electron rich nature and there will be bond formation between electron deficient and electron rich centers (Lewis acid–base concept). Pi-electronic cloud of benzene ring also form interactions with positively charged heavy metals due to cation-π interaction. Carboxyl group of HCP-AA after ionization form interactions with positively charged heavy metal ions. HCP-AA has porous surface so diffusion of heavy metals also takes place and it helps in adsorption of heavy metals. Reasonable surface area, narrow pore size distribution, hierarchical pore structure, accompanied by Lewis basic sites in HCP-AA are few of the desirable features for the study of heavy metal uptake where sorption isotherms measured at 273 K and 1 bar. The detailed mechanism of Cr^{3+} adsorption on the surface of HCP-AA is given in Fig. 14.

Effect of particle size of HCP-AA on heavy metal adsorption
The HCP-AA was transformed into powdered form using a pestle mortar and subsequently separated through different mesh size screens to obtain distinct particle sizes: 0.5 mm and 1 mm. Initial experiments revealed that the HCP-AA particles with a size of 0.5 mm exhibited superior adsorption capabilities compared to those with
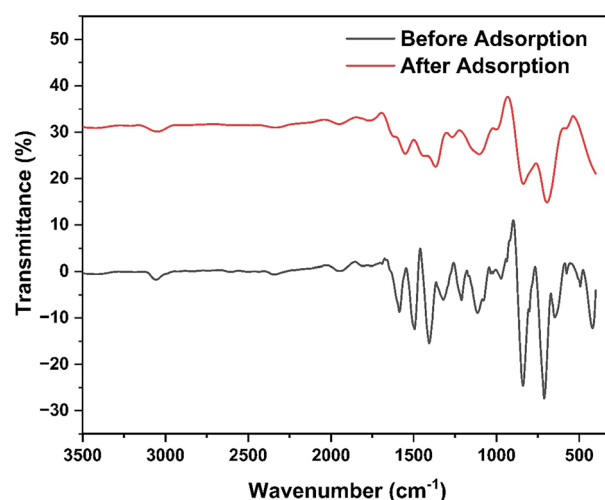

Figure 13. FTIR spectra of HCP-AA before and after an adsorption.
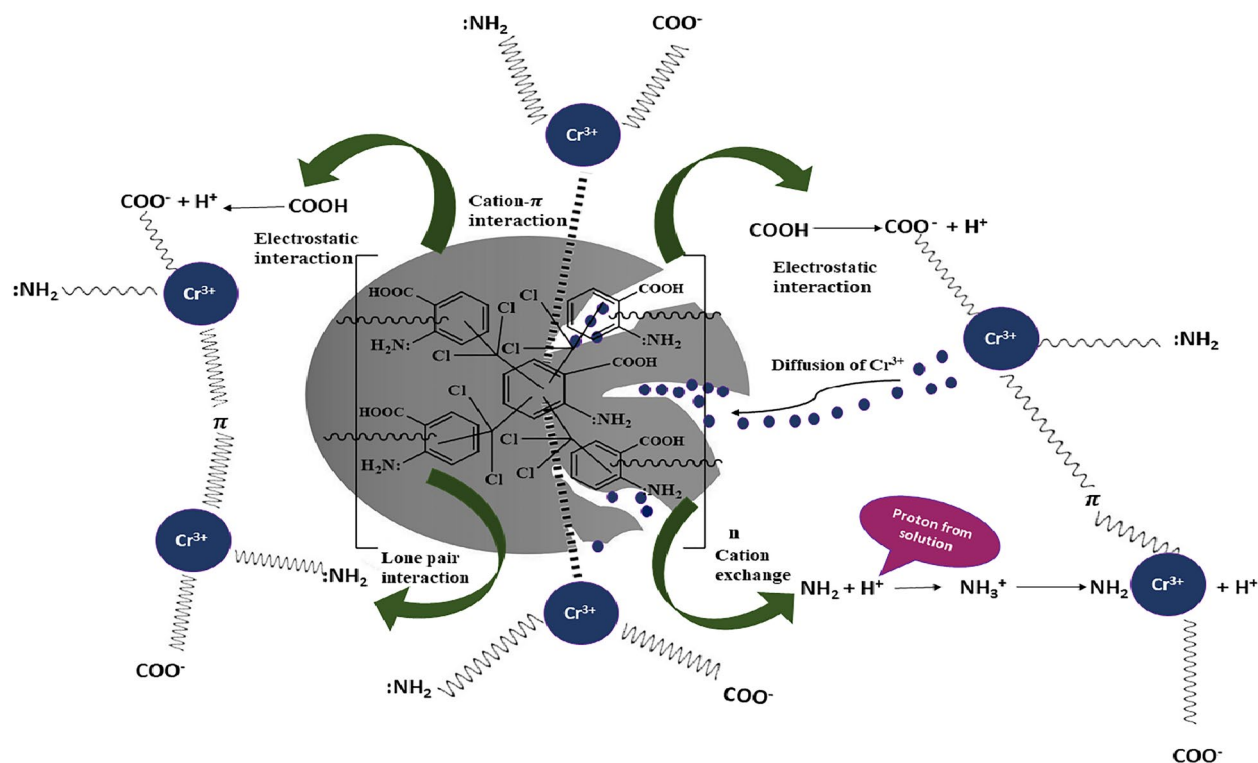
Figure 14. Mechanism for an adsorption of Cr^{3+} on surface of HCP-AA.

a 1 mm size. This can be attributed to the large surface area of the 0.5 mm particles. Given these findings, the 0.5 mm particle size was selected for subsequent experiments.

Point of zero charge (PZC)
The point at which surface of adsorbent has zero net charge, because the positive and negative charges are equal in numbers, this phenomenon is known as PZC. The aim of this PZC study was to investigate the pH at which the adsorbent surface exhibited an equal quantity of opposing ions and how adsorbent efficiency could be increased with the change of pH. A graph is produced between pHi and ΔpH to measure PZC[60]. Figure 15, displays the value of PZC, which was obtained from a line intersecting the x-coordinate. Trials for calculating PZC by using the salt addition technique revealed that at pH 4.0, the HCP-AA had a PZC.

Effect of wastewater pH
Results revealed that, pH of wastewater also affected the adsorption by HCP. In the experiment, the pH changed from acidic to basic (2–7) which showed that adsorption was not uniform throughout the pH changes. There will
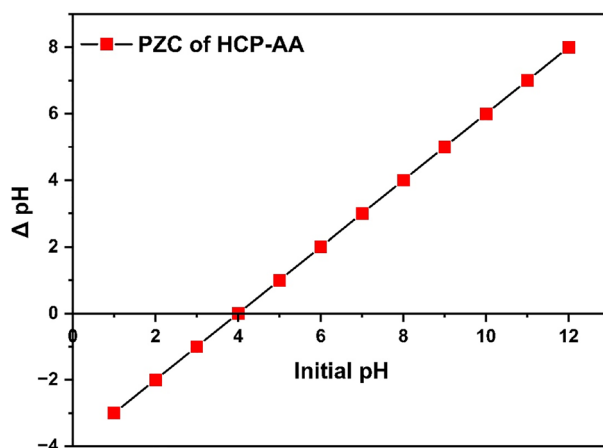

Figure 15. PZC of HCP-AA.

be a chance of precipitation of chromium ions at basic pH that is why the pH (2–7) was maintained for experiments to get reliable results[61]. The highest Cr^{3+} adsorption took place at pH 7. Adsorption increased as the pH increased from point of zero charge, because at high pH, negative charge on adsorbent become dominant that caused strong electrostatic interaction between negatively charged surface and positive metal ion. Therefore, we conclude that optimum pH for adsorption by HCP takes place at pH 7 as revealed in Fig. 16.

Effect of adsorbent dose on adsorption
Various quantities of HCP-AA, from 0.1 to 1.0 g, were tried and put into different flasks, containing 50 ml of the sample solution. Initially, the percentage removal of Cr^{3+} from water exhibited an upward trend as the quantity of adsorbent is raised (up to 0.8 g). The maximum Cr^{3+} removal was 93% at 0.8 g after this it became constant. This phenomenon may be due to the increased accessibility of active sites and a greater surface area when high dose of adsorbent was employed. A minor increase in removal efficiency after 0.8 g was because of equilibrium between the adsorbent HCP-AA and heavy metals. Therefore, we conclude that optimum quantity of adsorbent HCP-AA is 0.8 g, which is shown in Fig. 17.

Effect of contact time
This study was done by differing the time of contact for adsorption from 1 to 12 min while keeping all other factors constant. At first, the removal percentage was increase at rapid rate in first 6 min due to the abundance of available empty spaces. After that, the rate of adsorption slowed down because lesser sites were available for adsorption of Cr^{3+}. The maximum an adsorption took place at the time of 8 min, which was 93% and then became constant so, we conclude that optimum contact time for adsorption is 8 min as depicted in Fig. 18.
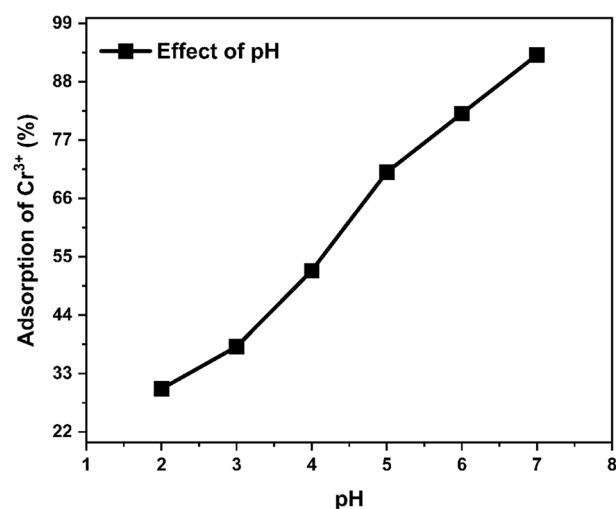

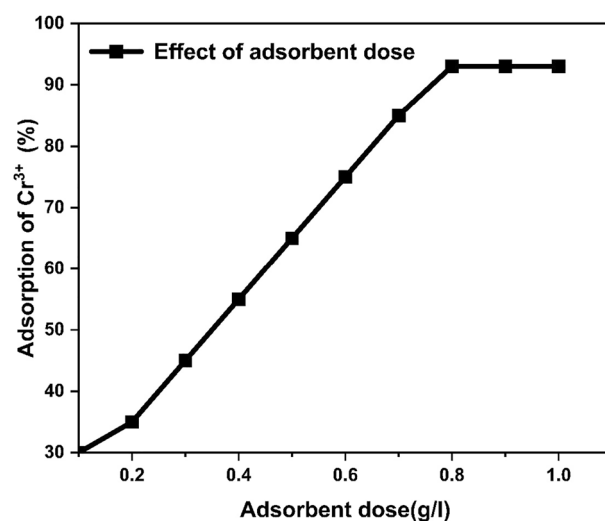**Figure 16.** Effect of pH on adsorption.
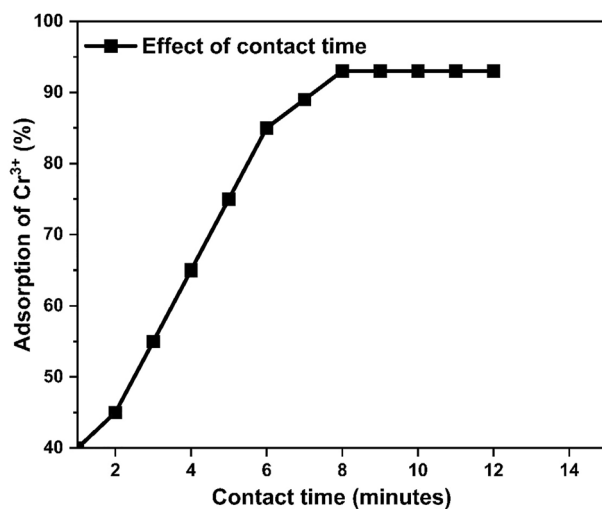

Figure 17. Effect of quantity of HCP-AA on adsorption.

Figure 18. Effect of contact time on adsorption.

Effect of temperature
The influence of temperature on uptake of Cr^{3+} onto surface of HCP-AA was examined in a range of temperatures, including 0–60 °C, while maintaining constant conditions of initial concentration 0.8 g/L, 12-min contact time, and a pH of 7.0. The findings revealed a proportional decrease in adsorption percentage with rising temperature, indicating an inverse correlation between temperature and the percentage removal of the heavy metals. Maximum adsorption occurred at lowest temperatures, resulting in a percentage removal variation from 92.6 to 59.7% within the temperature range of 283–333 K. These results are visually presented in Fig. 19. The enhanced adsorption process at minimum temperatures attributed to an augmentation in binding sites on the surface of HCP-AA.

Adsorption isotherms
Langmuir isotherm
The Langmuir isotherm parameters are shown in Table 3. The parameter RL revealed an adsorption is favorable for these metals ions. These parameters were calculated by using the following relation;

$$RL = \frac{1}{1 + b \cdot q_m} \tag{2}$$

The RL value is between 0 and 1 which confirms the successful uptake of Cr^{3+}. The Langmuir adsorption isotherm that is shown in Fig. 20 is excellent model to study monolayer adsorption and is mostly applied to find adsorption parameters for studies.

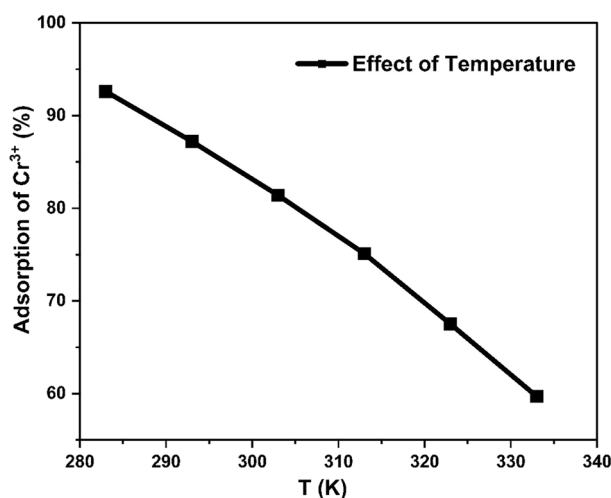The linear form of the Langmuir equation is shown in Eq. (3).

Figure 19. Effect of temperature on adsorption.

No. of experiment	C_o (mg/L)	C_e (mg/g)	$1/C_e$	Q_e (mg/g)	$1/Q_e$
1	5	2.38	0.42017	3.486429	0.286826
2	10	8.7	0.11494	6.832143	0.146367
3	20	13.25	0.07547	13.8125	0.072398
4	50	52.84	0.01893	33.82714	0.029562
5	100	59.68	0.01676	69.29714	0.014431
6	150	63.27	0.01581	104.8832	0.009534

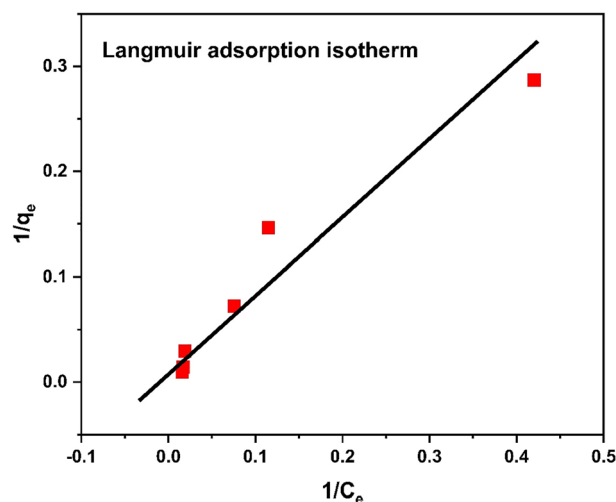**Table 3.** Langmuir Isotherm data for chromium metal.

Figure 20. Langmuir isotherm for chromium metal.

$$\frac{P_e}{q_e} = \frac{1}{q_{m \cdot b}} = \frac{P_e}{q_m} \tag{3}$$

The resulted data were well fitted by using Langmuir isotherm model[62].

Freundlich isotherm
From the data obtained from Freundlich adsorption isotherm which is reported in Table 4 shows that $1/n = 0.731$ while $n = 1.37$ shows an adsorption of Cr^{3+} is favorable.

Mathematical form of the Freundlich isotherm equation is given below;

$$Q_e = K_f C_e^{\frac{1}{n}} \tag{4}$$

The Freundlich isotherm's linear form is given here;

$$\log Q_e = \log K_f + \frac{1}{n} \log C_e \tag{5}$$

The Freundlich adsorption isotherm graph is shown in Fig. 21.

No. of experiment	C_o (mg/L)	C_e (mg/g)	Log C_e	Q_e (mg/g)	Log Q_e
1	5	2.38	0.3765	3.486429	0.5424
2	10	8.7	0.9395	6.832143	0.8346
3	20	13.25	1.1222	13.8125	1.1403
4	50	52.84	1.7229	33.82714	1.5293
5	100	59.68	1.7758	69.29714	1.8407
6	150	63.27	1.8012	104.8832	2.0208

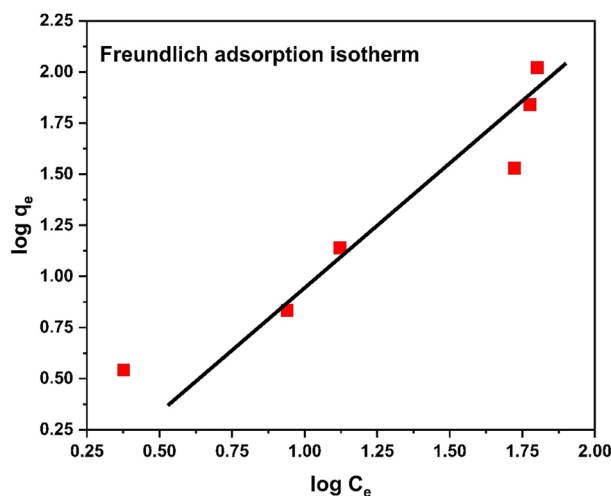**Table 4.** Experimental data of Freundlich isotherm.

Figure 21. Freundlich Isotherm.

Temkin isotherm

Temkin isotherm experimental analysis is shown in the Table 5. The R^2 value of Temkin isotherm is 0.6654, which shows that this adsorption is favorable.

Mathematical form of Temkin isotherm model is following

$$Q_e = RT/b \times \ln(A_r C_{aq}) \tag{6}$$

Linear form of the Temkin model

$$Q_e = B_1 \log K_t + B_1 \log C_e \tag{7}$$

The Temkin adsorption isotherm graph is shown in Fig. 22.

Dubinin Radushkevich isotherm

Employing the Dubinin–Radushkevich isotherm, the mechanism of adsorption is expressed through Gaussian energy distribution onto a heterogeneous surface of the adsorbent.

$$q_e = (q_s) \exp(-K_{ad}\varepsilon^2) \tag{8}$$

$$\ln q_e = \ln(q_s) - (K_{ad}\varepsilon^2) \tag{9}$$

where q_e, q_s, K_{ad}, ε are

- q_e = amount of an adsorbate in the adsorbent at the equilibrium(mg/g);
- q_s = theoretical isotherm saturation capacity (mg/g);
- K_{ad} = Dubinin–Radushkevich isotherm constant (mol^2/kJ^2) and
- ε = Dubinin–Radushkevich isotherm constant[63].

This model aids in differentiating between the physical and chemical adsorption of heavy metal ions to calculate the mean free energy E per molecule of adsorbate.

No. of Experiment	C_o (mg/L)	C_e (mg/g)	Log C_e	Q_e (mg/g)
1	5	2.38	0.3765	3.486429
2	10	8.7	0.9395	6.832143
3	20	13.25	1.1222	13.8125
4	50	52.84	1.7229	33.82714
5	100	59.68	1.7758	69.29714
6	150	63.27	1.8012	104.8832

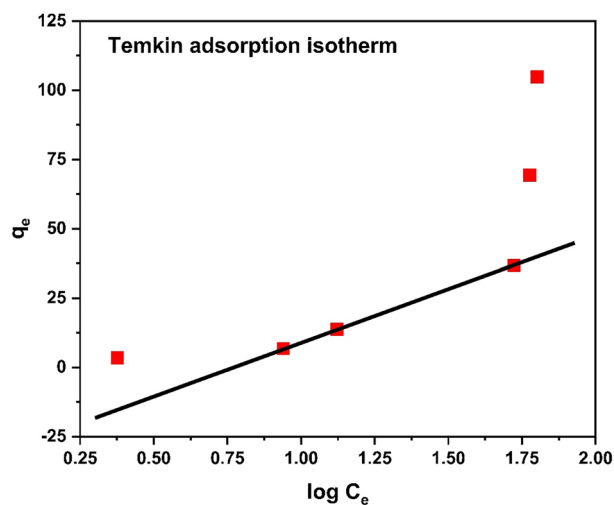**Table 5.** Experimental data of Temkin isotherm.

Figure 22. Temkin Isotherm.

$$E = 1/\sqrt{2B_{\mathrm{DR}}} \tag{10}$$

In the meantime, the value of ε can be determined as follows:

$$\varepsilon = \mathrm{RTln}[1 + 1/\mathrm{Ce}] \tag{11}$$

where Ce, T, and R stand for the adsorbate equilibrium concentration (mg/L), absolute temperature (K), and gas constant (8.314 J/mol K), respectively. The Dubinin-Radushkevich isotherm model is well known for the identification of its temperature-dependent feature, which is demonstrated when adsorption data at various temperatures are plotted as a function of the amount-adsorbed logarithm. $\ln q_e$ versus ε^2 that is shown in Fig. 23, ε^2 is the square of potential energy, all suitable data will lie on the same curve, named as the characteristic curve. The constants such as q_s, and K_{ad} were calculated from the appropriate plot using equation No. 11[63]. From the linear plot of DRK model, q_s was determined to 55.3 mg/g, the mean free energy, E = 0.7 kJ/mol indicates a physiosorption process with the *R^2 = 0.5125*.

The comparison of isotherms parameters is illustrate in Table 6. The above data revealed that the adsorption can be best explained by Freundlich adsorption isotherm with R^2 = 0.9273. Study of isotherms revealed multilayer adsorption and adsorption capacity increases with increase in concentration of chromium ions. However close R^2-value of Langmuir to Freundlich indicated monolayer adsorption with q_{max} of 52.63 mg/g, which confirm heterogeneous nature of adsorbent surface.
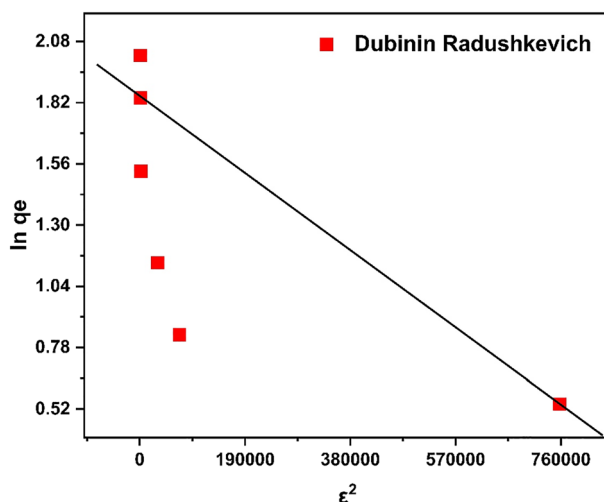

Figure 23. Dubinin Radushkevich Isotherm.

Adsorption isotherms	R^2	Other parameters	
Langmuir	0.91	q_m(mg/g)	69.67
		K_L (L/g)	0.013
Freundlich	0.9273	N	1.036
		1/n	0.965
		K_f	1.183
Temkin	0.6654	B_t	56.34
		K_t	0.250

Table 6. Comparison of adsorption isotherm parameters.

Kinetics study
Rate of adsorption was determined through kinetics study, which is discussed below, and it showed that an adsorption is well fitted with a pseudo second order model.

Pseudo first order reaction
Linear equation of pseudo first order reaction is as follow

$$\log (Q_e - Q_t) = \log Q_e - (k_1/2.302) \times t \tag{12}$$

where Q_e is equilibrium concentration, Q_t is adsorption concentration at the time t and K is constant. Figure 24 describes the pseudo first kinetic model of adsorbent towards adsorption.

Pseudo second order reaction
Equation of the pseudo second order reaction is given below

$$Q_t = q_e^2 K_2 t / 1 + q_e K_2 t \tag{13}$$

Figure 25 describes a pseudo second kinetic model behavior of adsorbent towards the adsorption.

Intraparticle diffusion model
Weber and Morris present an intraparticle diffusion model for finding out the adsorption process's diffusion mechanism and rate-controlling phase. This model's mathematical representation is as follows:

$$qt = Kidt^{0.5} + I \tag{14}$$

where I is the layer's thickness, qt(mg/g) is the amount of adsorbate adsorbed at time "t" and kid is intra-particle diffusion constant. The plot produced by the data is linear, a value of regression coefficient, is 0.9582[64]. The value of Kdiff is 0.1052 and thickness of layer on surface of HCP-AA is 0.1186. The graph between $t^{1/2}$ and q_t is shown in Fig. 26.

According to the comparative study it is observed that pseudo second order model is fit the best with R^2 = 0.979 as compares to pseudo 1st order kinetics model. The second order kinetic model predicts chemical adsorption of Cr^{3+} on surface of polymer. The 1st order kinetic model's regression "R^2" value "0.601" is lower than the
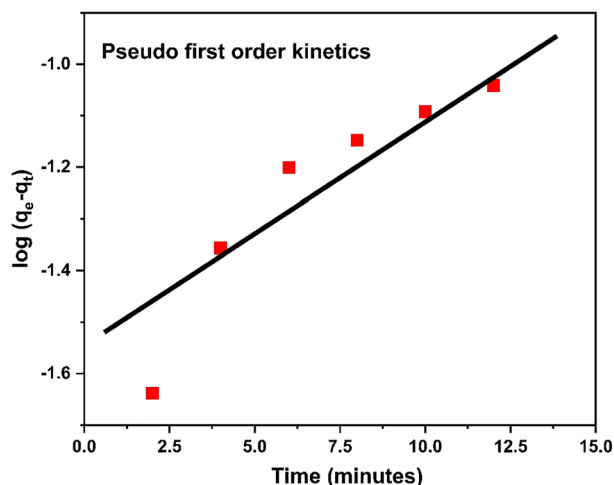

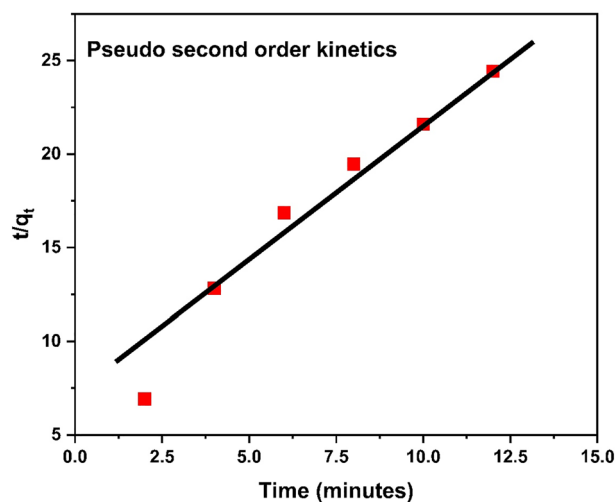**Figure 24.** Pseudo first order kinetics graph.

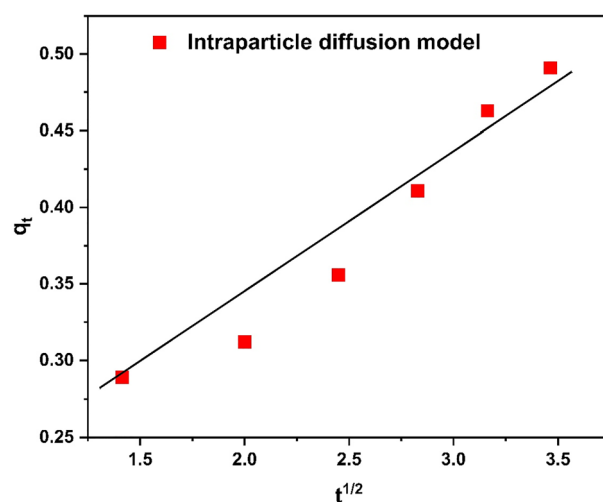**Figure 25.** Pseudo second order kinetics graph.

Figure 26. Intraparticle diffusion model.

2nd order kinetic model's R^2 value 0.979. Additionally, q_e calculated (0.601 mg g^{-1}) value from Eq. 8 and 9 is closer to q_e experimental value (0.589 mg g^{-1}) as shown in Table 7. Therefore, second order kinetic model is the best to examine the kinetic constants of Cr^{3+} adsorption on surface of HCP-AA. Comparative data analysis is shown in Table 7.

Thermodynamics study
The determination of heat changes in a system, or its state, can be described using various state functions, such as the Gibbs free energy (ΔG), an entropy (ΔS), and the enthalpy (ΔH). These parameters offer insights into the mechanism of the adsorption, distinguishing between exothermic and endothermic reactions. The thermodynamic relationships can be expressed through the equation:

$$\ln K_c = (\Delta S/R) - (\Delta H/RT) \tag{15}$$

Sr. No	Order of reaction	Intercept	R²	Qe exp	Qe cal	K
1	Pseudo first order	− 1.589	0.861	0.589	0.023	K_1 (min^{-1}) = 0.125
2	Pseudo second order	5.536	0.979	0.589	0.601	K_2 (gmol^{-1} min^{-1}) = 0.52

Table 7. Comparison of kinetics graph.

here

- ΔS represents entropy (indicating degree of randomness),
- ΔH denotes enthalpy
- T is a temperature in Kelvin
- K_c is an equilibrium constant

An equilibrium constant (K_c) is defined as the ratio of a amount of heavy metal adsorbed on surface of HCP-AA at the equilibrium (C_a) to equilibrium concentration of a heavy metal in the solution (C_e), as given by:

$$K_c = C_a/C_e \qquad (16)$$

In exothermic processes, the Gibbs free energy (ΔG^0), a entropy (ΔS^0), and the enthalpy (ΔH^0) exhibit negative values, governed by the relationship:

$$\Delta G^0 = \Delta H^0 - T\Delta S^0 \qquad (17)$$

Negative enthalpy and entropy value signify the exothermic nature of the reaction, suggesting an inverse relationship with temperature. As temperature increases, adsorption tends to decrease, and vice versa. The graph between ln Kc versus $1/T$ for the adsorption of chromium over HCP-AA is illustrated in Fig. 27. The value for adsorption enthalpy (ΔH^0) was -60.91 kJ/mol and adsorption entropy (ΔS^0) was -45.79 kJ/mol K which were calculated from plot. The resulting values for Gibbs free energy (ΔG^0) are presented in Table 8. The Positive ΔG^0 suggests the non-spontaneous nature of a process. A rise in the ΔG^0 values with increase in temperature shows adsorption is unfavorable at the higher temperatures. A negative ΔH_0 value implies that the adsorption of Cr^{3+} is exothermic, while the negative ΔS^0 value shows a reduction in unpredictability at the contact between the adsorbent-adsorbate during the adsorption.

The adsorption capacity of HCP-AA in relation to other comparable adsorbents is displayed in Table 9. It shows 52.63 mg/g adsorption capacity of HCP-AA that is due to is high surface area, porous surface and active functional groups.

Application of HCP-AA for CO₂ uptake
Pure CO_2 gas was provided through a cylinder, connected with a heater. The pressure and temperature of gas was controlled till it was transferred to reactor containing adsorbent (HCP-AA) for the adsorption experiment.
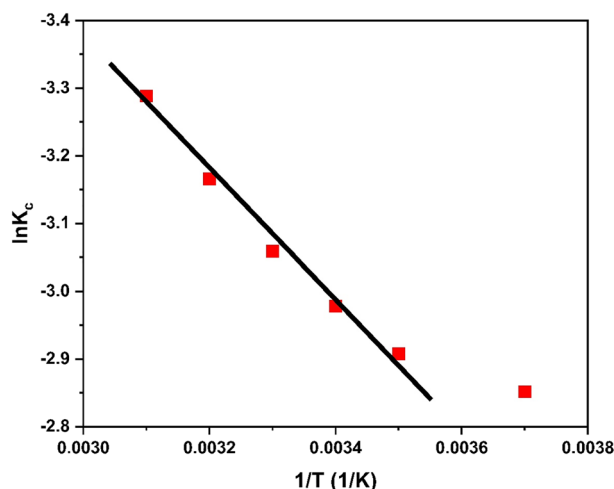

Figure 27. Graph of thermodynamics study.

T (K)	1/T (1/K)	C_e	K_c	lnK_c	ΔG (KJ/mol)	ΔS (J/mol k)
283	0.0037	0.76	0.05775	-2.8516	6.5880	-0.238
293	0.0035	1.28	0.05459	-2.9079	7.0836	-0.232
303	0.0034	1.86	0.05087	-2.9784	7.5030	0.226
313	0.0033	2.49	0.04693	-3.0591	7.9606	-0.220
323	0.0032	3.25	0.04218	-3.1658	8.5015	-0.213
333	0.0031	4.03	0.03731	-3.2884	9.1041	-0.210

Table 8. Thermodynamics study of adsorption.

Material	Q_{max} (mg/g)	References
SAM-HCPs	51	[65]
FIR-54	53.2	[66]
PEI/ECs	36.8	[67]
HCPs-N	44.5	[68]
PVIm-6-SCD	236.8	[69]
MC-N	14.8	[70]
HCP-AA	52.63	This work

Table 9. Comparison of HCP-AA with other adsorbents for chromium removal.

The electrical heater was used to heat the reactor and thermocouple was used to regulate the temperature. Temperature and pressure of CO_2 were determined at 273 and 298 K by using thermocouple and pressure gauge connected to the computer respectively. Nitrogen gas was used for as an inert medium for discharging and cleaning of mixing tank represented in Fig. 28[71].

Mechanism of adsorption of CO_2
The HCP-AA showing high BET surface area, abundant pores, carboxyl (-COOH) and amino (–NH_2) group surged us to investigate their CO_2 adsorption properties. Nitrogen rich HCPs were used extensively for the CO_2 adsorption because of polymers host–guest chemistry.

There are two ways that HCP-AA can adsorb CO_2: first, the amine group adsorbed the CO_2 molecules by the creation of a zwitterion intermediate (R–$NH^{+2-}COO^-$). A zwitterion intermediate then donates its H^+ to the nearby amine group to generate ammonium-carbamate ion pairs ((R–NH^{3+}–COO–NH–R)), and intermolecular H^+ transfer can also form carbamic acid (R–NH–COOH) species[72]. General mechanism for the CO_2 adsorption by HCP-AA through chemisorption is shown in Fig. 29.

CO_2 adsorption
A CO_2 adsorption study of HCP-AA were conducted at 273 and 298 K is shown in Fig. 30. The adsorption isotherms demonstrating the HCP-AA ability to the CO_2 uptake at various temperatures.

Quantity of CO_2 adsorbed on surface of HCP-AA is directly related to pressure applied. As, we increased pressure, the quantity of CO_2 adsorbed increased as shown in Fig. 30. HCP-AA adsorbed 31.1 cm^3/g CO_2 at pressure 850 mmHg at 273 K but at temperature 298 K, it adsorbed 25.2 cm^3/g at 850 mmHg. The adsorption capacity of the HCP-AA for CO_2 was a 1.39 mmol/g at 273 K and 1.12 mmol/g at 298 K, which is calculated by using a following relation.

$$\text{Adsorption capacity } = \text{ moles of } CO_2 \text{adsorbed/mass of adsorbent in grams } \times \text{ 1000} \tag{18}$$

It showed a maximum CO_2 uptake ability of 6.1 wt% at 273 K and 5 wt% at 298 K was because of its high surface area, abundant amino and the carboxyl groups as shown in Fig. 31. The CO_2 uptake ability reduced at higher temperatures.

To clarify the interaction of HCP-AA with CO_2 molecule, the isosteric heat was estimated by using Clausius–Clapeyron equation. The Q_{st} of the HCP-AA (29.2–25.4 kJ mol^{-1}) which is shown in Fig. 32 is because of tightly packed porous structure and nitrogen content.
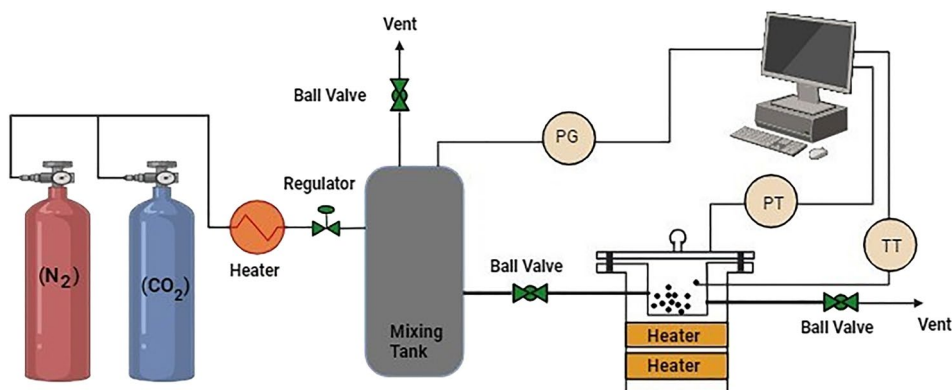

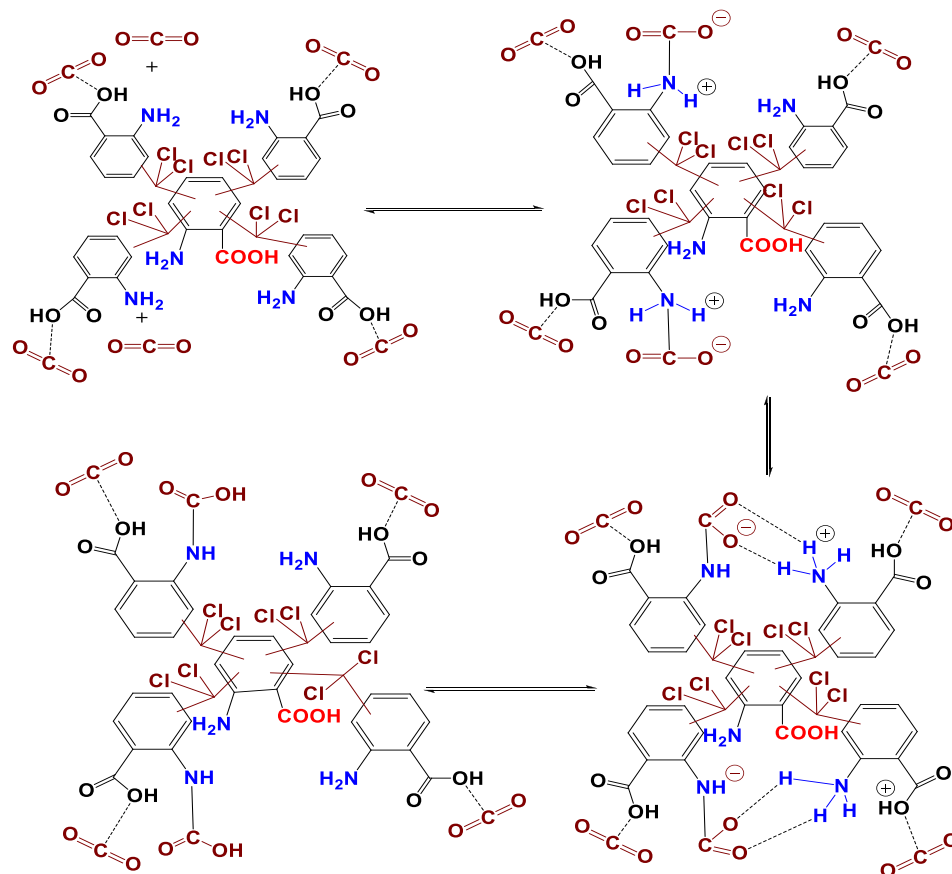**Figure 28.** Instrumentation of CO_2 adsorption setup.

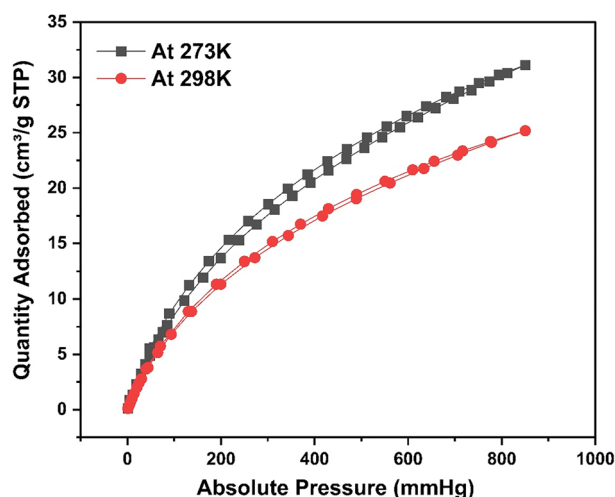**Figure 29.** Mechanism of adsorption of CO_2 on HCP-AA.

Figure 30. Effect of pressure on quantity of CO_2 adsorbed (cm^3/g).

A comparison of CO_2 uptake capacity of HCP-AA with other similar adsorbents at 1 bar pressure is shown in Table 10. It shows the adsorption capacity of 1.39 and 1.12 mmol/g at 273 K and 298 K, respectively, which is due to the high surface area, porous surface and the nitrogen content.

Reusability of HCP-AA for Cr^{3+} and CO_2 uptake
For industrial applications, reusability is the important attribute due to economic value. Conducting repeated adsorption on the same HCP-AA up to 10 cycles reveal that there is a minimal decrease in its efficiency till 3
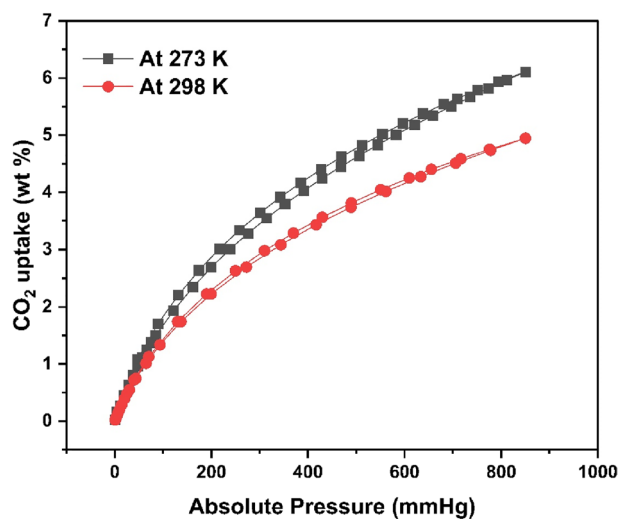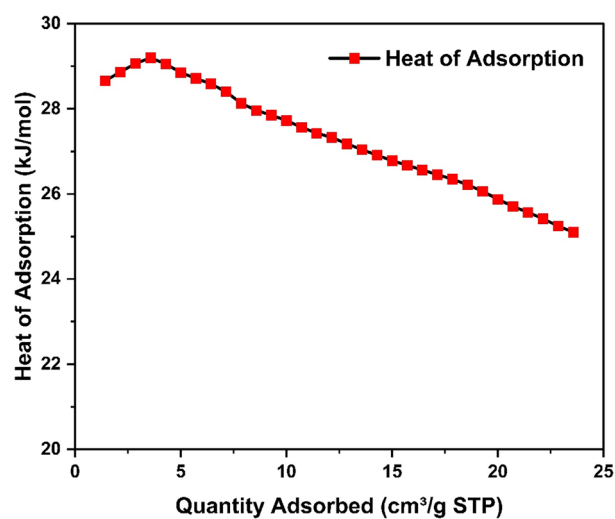
Figure 31. Effect of pressure on CO_2 uptake (wt%).

Figure 32. Heat of adsorption of HCP-AA for different quantities of CO_2.

Adsorbents	CO_2 uptake capacity (mmol/g)	Temperature (K)	Pressure (bar)	References
HPIM-1	1.73	298	1	[73]
KFUPM-1	1.04	298	1	[74]
HCP-MAAM-2	1.35	273	1	[50]
HCP-MAAM-3	1.28	273	1	[50]
y-POP	1.34	273	1	[75]
KFUPM-2	1.04	298	1	[76]
TPAC-HCP-4	0.9	273	1	[47]
TPE-CPOP1	0.89	298	1	[77]
man-Azo-P1	1.43	273	1	[78]
HCP-PN-1	1.63	273	1	[79]
HCP-PN-1	1.31	298	1	[79]
HCP-PN-2	1.11	273	1	[79]
HCP-PN-2	0.83	298	1	[79]
HCP-AA	1.39	273	1	This study
HCP-AA	1.12	298	1	This study

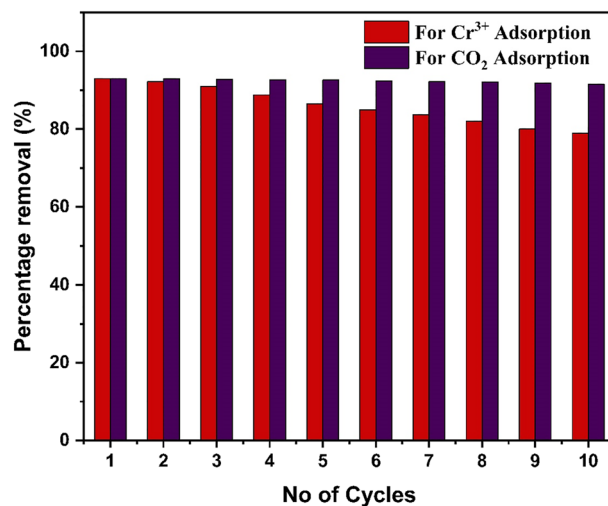**Table 10.** Comparison of HCP-AA performance with other adsorbents.

Figure 33. Reusability of HCP-AA for Cr^{3+} and CO_2 adsorption.

cycles after that HCP-AA start occupying with heavy metal ions so there is gradually decrease in its efficiency to adsorb further metal ions. For reuse of HCP-AA for several times acidic medium is provided to the HCP-AA by treated it with 0.1 molar HCl solution so desorption takes place but this can regenerate the capability of HCP-AA for some extent. The graph of effect of repeated adsorption experiment on adsorption is shown in Fig. 33. To study the adsorbents recyclability for CO_2 uptake, the ten adsorption cycles were performed at the 298 K and HCP-AA were recycled for 8 h at 410 K in a vacuum oven. The HCP-AA adsorption potential reduced by 1.5% after 10 cycles.

Conclusions and future perspectives
There is no life without plenty of fresh water and air, but due to industrialization and population bloom, clean sources of water are declining day-by-day and air is polluted with greenhouse gases like CO_2, which can result in global warming. The situation is getting worse in developing countries with few reservoirs of fresh water. One of the main cause of water pollution are heavy metals, which may cause fatal diseases in humans. Therefore, it is an ultimate need to purify water resources. HCPs are excellent candidates to clean water and air through their adsorption capacities as per their structural features like porosity and high surface area. In this article, a simple approach for the synthesis of hyper cross-linked polymer (HCP-AA) through Friedel–Crafts reaction and its use for sequestration of CO_2 and Cr^{3+} metal ions with potent results are reported. The produced HCP-AA contains oxygen and nitrogen, which gives them a great selectivity and high adsorption capacity for the pollutants along with high stability and reusability. The designed HCP-AA can be a good candidate to solve today's world problems like global warming and water scarcity. In near future, HCPs have the potential to use in industries and powerhouses, where significant amount of heavy metals, dyes and CO_2 are emitted. In order to keep environment clean and safe it is better to use such types of HCPs, before the release above-mentioned environmental pollutants to the environment. In order to make it more effective, further work is required to make such HCPs synthesis more feasible, optimized, efficient, and cost effective.

Data availability
The datasets used and analyzed in this research are available from corresponding author upon request.

References
1. Amonovich, M. R. & Ahroro'g'li, N. S. Importance of water for living organisms and national economy, physical and chemical methods of wastewater treatment. *Am. J. Res. Human. Soc. Sci.* **9**, 7–13 (2023).
2. Pierrat, E. *et al.* Global water consumption impacts on riverine fish species richness in life cycle assessment. *Sci. Total Environ.* **854**, 158702 (2023).
3. Jeelani, G., Lone, S. A., Lone, A. & Deshpande, R. D. Groundwater resource protection and spring restoration in Upper Jhelum Basin (UJB), western Himalayas. *Groundw. Sustain. Dev.* **15**, 100685 (2021).
4. Kılıç, Z. The importance of water and conscious use of water. *Int. J. Hydrol.* **4**, 239–241 (2020).
5. Zhang, Y. *et al.* Importance and vulnerability of lakes and reservoirs supporting drinking water in China. *Fundam. Res.* **3**, 265–273 (2023).
6. Mishra, R. K. Fresh water availability and its global challenge. *Br. J. Multidiscip. Adv. Stud.* **4**, 1–78 (2023).
7. Sadighara, P. *et al.* Association between non-alcoholic fatty liver disease and heavy metal exposure: A systematic review. *Biol. Trace Elem. Res.* **201**(12), 5607–5615 (2023).
8. Albayrak, L., Türksoy, V. A., Khalilov, R. & Eftekhari, A. Investigation of heavy metal exposure and trace element levels in acute exacerbatıon of COPD. *J. King Saud Univ.-Sci.* **35**, 102422 (2023).

9. Walsh, M. G. & Hossain, S. J. E. Population structure and diet generalism define a preliminary ecological profile of zoonotic virus hosts in the Western Ghats, India. *Epidemics* **33**, 100416 (2020).
10. Amato-Lourenço, L. F. *et al.* Presence of airborne microplastics in human lung tissue. *J. Hazard. Mater.* **416**, 126124 (2021).
11. Lin, X., Deng, Y.-Y., Zhang, Q., Han, D. & Fu, Q. J. M. Effect of POSS size on the porosity and adsorption performance of hybrid porous polymers. *Macromolecules* **56**, 1243–1252 (2023).
12. Zhang, S. *et al.* Efficient photocatalytic hydrogen evolution: Linkage units engineering in triazine-based conjugated porous polymers. *J. Colloid Interface Sci.* **637**, 41–54 (2023).
13. Jethave, G., Fegade, U., Rathod, R. & Pawar, J. Dye pollutants removal from waste water using metal oxide nanoparticle embedded activated carbon: An immobilization study. *J. Dispers. Sci. Technol.* **40**, 563–573 (2019).
14. Shen, Y., Ni, W.-X. & Li, B. Porous organic polymer synthesized by green diazo-coupling reaction for adsorptive removal of methylene blue. *ACS Omega* **6**, 3202–3208 (2021).
15. Huang, L. *et al.* Selective recovery of Gd (III) by benzimidazole-and benzoxazole-linked 3D porous polymers. *J. Water Process Eng.* **51**, 103378 (2023).
16. Liao, Q. *et al.* Rational design of hyper-crosslinked polymers for biomedical applications. *J. Polym. Sci.* https://doi.org/10.1002/pol.20230270 (2023).
17. Huang, J. & Turner, S. Hypercrosslinked polymers: A review. *Polym. Rev.* **58**(1), 1–41 (2018).
18. Guo, Y. *et al.* Adsorption behaviors and mechanisms of porous hypercrosslinked polymers with adjustable functional groups toward doxycycline hydrochloride from water. *J. Appl. Polym. Sci.* **141**, e54818 (2024).
19. Feng, X., Wei, L., Liu, Y., Chen, X. & Tian, R. Orchestrated strategies for developing fluorophores for NIR-II imaging. *Adv. Healthc. Mater.* **12**, 2300537 (2023).
20. Giri, A., Sahoo, A., Dutta, T. K. & Patra, A. Cavitand and molecular cage-based porous organic polymers. *ACS Omega* **5**, 28413–28424 (2020).
21. Raza, S., Nazeer, S., Abid, A. & Kanwal, A. Recent research progress in the synthesis, characterization and applications of hyper cross-linked polymer. *J. Polym. Res.* **30**, 415. https://doi.org/10.1007/s10965-023-03783-7 (2023).
22. Zhang, Q. *et al.* Linking electron-rich Pillar [5] arene into hyper-cross-linked polymers for highly effective adsorption of iodine vapor. *J. Solid State Chem.* **331**, 124528 (2024).
23. Raza, A. *et al.* Recent advances in carbonaceous sustainable nanomaterials for wastewater treatments. *Sustain. Mater. Technol.* **32**, e00406 (2022).
24. Meng, Q. *et al.* Synthesis of hypercross-linked hybrid polyanilines from hollow spherical polyaniline and octavinylsilsesquioxane and its dye adsorption performance. *Mater. Today Commun.* **34**, 105488 (2023).
25. Laabd, M. *et al.* Efficient detoxification of Cr (VI)-containing effluents by sequential adsorption and reduction using a novel cysteine-doped PANi@ faujasite composite: Experimental study supported by advanced statistical physics prediction. *J. Hazard. Mater.* **422**, 126857 (2022).
26. Liao, X. *et al.* Synergistic catalysis of hypercrosslinked ionic polymers with multi-ionic sites for conversion of CO2 to cyclic carbonates. *Mol. Catal.* **535**, 112834 (2023).
27. Hao, A., Fu, Z., Huang, J. J. S. & Technology, P. Acrylate-functionalized hyper-cross-linked polymers: Effect of the porogens in the polymerization on their porosity and adsorption from aqueous solution. *Sep. Purif. Technol.* **311**, 123380 (2023).
28. Wang, Y., Yang, N., Soldatov, M., Liu, H. J. R. & Polymers, F. A novel phosphazene-based amine-functionalized porous polymer with high adsorption ability for I2, dyes and heavy metal ions. *React. Funct. Polym.* **173**, 105235 (2022).
29. Chenarani, B., Rahnama Haratbar, P. & Ghaemi, A. Removal of diclofenac sodium pollutant from drug contaminants using a hyper-cross-linked polymer adsorbent. *Iran. Polym. J.* **31**, 1459–1473 (2022).
30. Wang, C. *et al.* Preparation of amino-functionalized triazine-based hyper-crosslinked polymer for efficient adsorption of endocrine disruptors. *Talanta* **266**, 125142 (2024).
31. Li, M. *et al.* Facile synthesis of magnetic hypercrosslinked polymer for the magnetic solid-phase extraction of benzoylurea insecticides from honey and apple juice samples. *Food Chem.* **395**, 133596 (2022).
32. Chanchaona, N. & Lau, C. H. Assessing the environmental impacts of flow and batch syntheses of hypercrosslinked polymers for low-pressure CO2 adsorption. *Sep. Purif. Technol.* **329**, 125145 (2023).
33. He, X. *et al.* D-type neuropeptide decorated AIEgen/RENP hybrid nanoprobes with light-driven ROS generation ability for NIR-II fluorescence imaging-guided through-skull photodynamic therapy of gliomas. *Aggregate* **5**(1), e396 (2023).
34. Huang, X. *et al.* Facile preparation of hierarchical AgNP-loaded MXene/Fe3O4/polymer nanocomposites by electrospinning with enhanced catalytic performance for wastewater treatment. *ACS Omega* **4**, 1897–1906 (2019).
35. Liao, G. *et al.* Direct synthesis of hypercrosslinked microporous poly (para-methoxystyrene) for removal of iron (III) ion from aqueous solution. *Microporous Mesoporous Mater.* **307**, 110469 (2020).
36. Rahnama Haratbar, P., Nasiri, M. & Ghaemi, A. Hypercrosslinked polystyrene-based adsorbents for the removal of lead ions from aqueous effluents: Experimental and RSM modeling. *Iran. Polym. J.* **32**, 929–946 (2023).
37. Masoumi, H., Ghaemi, A. & Gilani, H. G. Exploiting the performance of hyper-cross-linked polystyrene for removal of multi-component heavy metal ions from wastewaters. *J. Environ. Chem. Eng.* **9**, 105724 (2021).
38. Masoumi, H., Ghaemi, A., Ghanadzadeh Gilani, H. & Ramazanipour Penchah, H. Benzene-based hypercross-linked polymers as a highly efficient adsorbent for cadmium removal from aqueous solution. *Int. J. Environ. Sci.* https://doi.org/10.1007/s13762-021-03798-x (2022).
39. Wang, L. *et al.* Multifunctional nanomicelles constructed via an aggregation and de-aggregation strategy for magnetic resonance/NIR II fluorescence imaging-guided type I photodynamic therapy. *Mater. Chem. Front.* **7**, 3657–3667 (2023).
40. James, A. M. *et al.* Selective environmental remediation of strontium and cesium using sulfonated hyper-cross-linked polymers (SHCPs). *ACS Appl. Mater. Interfaces* **11**, 22464–22473 (2019).
41. Anito, D. A., Wang, T.-X., Liu, Z.-W., Ding, X. & Han, B.-H. Iminodiacetic acid-functionalized porous polymer for removal of toxic metal ions from water. *J. Hazard. Mater.* **400**, 123188 (2020).
42. Wang, X. *et al.* Phenolic hydroxyl-functionalized hyper-cross-linked polymers for efficient adsorptive removal of aniline. *Sep. Purif. Technol.* **305**, 122443 (2023).
43. Podkościelna, B., Kołodyńska, D. & Podkościelny, P. J. A. Chemical modification of commercial St-DVB microspheres and their application for metal ions removal. *Adsorption* **25**, 529–544 (2019).
44. Gao, H. Synthesis of linear polymers in high molecular weights via reaction-enhanced reactivity of intermediates using friedel-crafts polycondensation. *ACS omega* **6**, 4527–4533 (2021).
45. Aljboar, M. T. *et al.* Synthesis of poly (aniline-co-benzene)-based hypercrosslinked polymer for Hg (II) ions removal from polluted water: kinetic and thermodynamic studies. *Water* **15**, 3009 (2023).
46. Liu, M., Shao, L., Huang, J., Liu, Y.-N.J.M. & Materials, M. O-containing hyper-cross-linked polymers and porous carbons for CO2 capture. *Microporous Mesoporous Mater.* **264**, 104–111 (2018).
47. Shao, L. *et al.* One-step synthesis of N-containing hyper-cross-linked polymers by two crosslinking strategies and their CO2 adsorption and iodine vapor capture. *Sep. Purif. Technol.* **262**, 118352 (2021).
48. Shao, L., Wang, S., Liu, M., Huang, J. & Liu, Y.-N. Triazine-based hyper-cross-linked polymers derived porous carbons for CO2 capture. *Chem. Eng. J.* **339**, 509–518 (2018).

49. Chanchaona, N., Lau, C. H. J. S. & Technology, P. Assessing the environmental impacts of flow and batch syntheses of hyper-crosslinked polymers for low-pressure CO2 adsorption. *Sep. Purif. Technol.* **329**, 125145 (2024).
50. Fayemiwo, K. A. *et al.* Nitrogen-rich hyper-crosslinked polymers for low-pressure CO2 capture. *Chem. Eng. J.* **334**, 2004–2013 (2018).
51. Sadak, A. E., Cucu, E., Hamur, B., Ün, İ & Altundas, R. Cyclotriphosphazene and tricarbazole based microporous hyper-crosslinked conjugated polymer for CCUS: Exceptional CO2 selectivity and high capacity CO2, CH4, and H2 capture. *J. CO2 Util.* **67**, 102304 (2023).
52. Karami, B., Bayat, B., Penchah, H. R. & Ghaemi, A. J. F. Nanoporous hypercrosslinked polymers as cost-effective catalysts to significantly promote the CO2 absorption performance of water-lean solvents for post-combustion CO2 capture. *Fuel* **363**, 130929 (2024).
53. Li, S., Zhan, Z., Wang, X. & Tan, B. J. P. C. Synthesis of hypercrosslinked polymers with a spherical shell structure for highly effective cycloaddition of CO2 under ambient conditions. *Polym. Chem.* **14**, 4362–4371 (2023).
54. Torkashvand, A., Moradi, M. R. & Ghaemi, A. Amine grafting of carbazole-based hypercrosslinked polymer as an adsorbent to enhance CO2 capture. *Case Stud. Chem. Environ. Eng.* **8**, 100472 (2023).
55. Song, W. *et al.* Green synthesis of hypercrosslinked polymers for CO2 capture and conversion: Recent advances, opportunities, and challenges. *Green Chem.* (2024).
56. Li, M. *et al.* A dual-ionic hyper-crosslinked polymer for efficient CO2 fixation and conversion. *Chem. Eng. J.* **481**, 148550 (2024).
57. Areej, I. *et al.* Fabrication of new hyper-cross-linked polymer for efficient heavy metal adsorption from industrial wastewater (2024).
58. Weng, T.-H. *et al.* Rationally engineered ultrastable three-dimensional (3D) conjugated microporous polymers containing triptycene, tetraphenylethene, and benzothiadiazole units as exceptional high-performance organic electrodes for supercapacitors. *ACS Appl. Energy Mater.* **6**, 9012–9024 (2023).
59. Gouda, A. A. *et al.* Preconcentration and separation of Cd (II), Co (II), Cu (II), Ni (II), and Pb (II) in environmental samples on cellulose nitrate membrane filter prior to their flame atomic absorption spectroscopy determinations. *Int. J. Environ. Anal. Chem.* **103**, 364–377 (2023).
60. Şenol, Z. M., Elma, E., El Messaoudi, N. & Mehmeti, V. Performance of cross-linked chitosan-zeolite composite adsorbent for removal of Pb2+ ions from aqueous solutions: Experimental and Monte Carlo simulations studies. *J. Mol. Liq.* **391**, 123310 (2023).
61. Merabet, S. & Boukhalfa, C. Chromium removal from aqueous solutions by co-precipitation with Al (III), Fe (III) and Al (III)/Fe (III) effect of pH and competitive ions. *J. Pharm. Biol. Chem. Sci.* **6**, 1715–1720 (2015).
62. Al-Qahtani, K. M. Water purification using different waste fruit cortexes for the removal of heavy metals. *J. Taibah Univ. Sci.* **10**, 700–708 (2016).
63. Şenol, Z. M., Keskin, Z. S. & Şimşek, S. Synthesis and characterization of a new hybrid polymer composite (pollene@ polyacrylamide) and its applicability in uranyl ions adsorption. *J. Radioanal. Nuclear Chem.* **332**, 2239–2248 (2023).
64. Şen, N. E. & Şenol, Z. M. Effective removal of Allura red food dye from water using cross-linked chitosan-diatomite composite beads. *Int. J. Biol. Macromol.* **253**, 126632 (2023).
65. Li, B. *et al.* Hypercrosslinked microporous polymer networks for effective removal of toxic metal ions from water. *Microporous Mesoporous Mater.* **138**, 207–214 (2011).
66. Fu, H.-R., Xu, Z.-X. & Zhang, J. Water-stable metal–organic frameworks for fast and high dichromate trapping via single-crystal-to-single-crystal ion exchange. *Chem. Mater.* **27**, 205–210 (2015).
67. Qiu, B. *et al.* Polyethylenimine facilitated ethyl cellulose for hexavalent chromium removal with a wide pH range. *ACS Appl. Mater. Interfaces* **6**, 19816–19824 (2014).
68. Liu, R. *et al.* Synthesis and facile functionalization of siloxane based hyper-cross-linked porous polymers and their applications in water treatment. *Eur. Polym. J.* **119**, 94–101 (2019).
69. Xie, Y. *et al.* Hypercrosslinked mesoporous poly (ionic liquid) s with high density of ion pairs: Efficient adsorbents for Cr (VI) removal via ion-exchange. *Chem. Eng. J.* **378**, 122107 (2019).
70. Qiu, B. *et al.* Cellulose derived magnetic mesoporous carbon nanocomposites with enhanced hexavalent chromium removal. *J. Mater. Chem. A* **2**, 17454–17462 (2014).
71. Ramezanipour Penchah, H., Ghaemi, A. & Ganadzadeh Gilani, H. Benzene-based hyper-cross-linked polymer with enhanced adsorption capacity for CO2 capture. *Energy Fuels* **33**, 12578–12586 (2019).
72. Moradi, M. R., Torkashvand, A., Ramezanipour Penchah, H. & Ghaemi, A. J. S. R. Amine functionalized benzene based hypercrosslinked polymer as an adsorbent for CO2/N2 adsorption. *Sci. Rep.* **13**, 9214 (2023).
73. Hu, Z., Wang, Y., Wang, X., Zhai, L. & Zhao, D. J. A. J. Solution-reprocessable microporous polymeric adsorbents for carbon dioxide capture. *AIChE J.* **64**, 3376–3389 (2018).
74. Abdelnaby, M. M. *et al.* Carbon dioxide capture in the presence of water by an amine-based crosslinked porous polymer. *J. Mater. Chem.* **6**, 6455–6462 (2018).
75. Kong, X., Li, S., Strømme, M. & Xu, C. J. N. Synthesis of porous organic polymers with tunable amine loadings for CO2 capture: Balanced physisorption and chemisorption. *Nanomaterials* **9**, 1020 (2019).
76. Abdelnaby, M. M. *et al.* A microporous organic copolymer for selective CO2 capture under humid conditions. *ACS Sustain. Chem. Eng.* **7**, 13941–13948 (2019).
77. Mohamed, M. G., Ahmed, M. M., Du, W.-T. & Kuo, S.-W.J.M. Meso/microporous carbons from conjugated hyper-crosslinked polymers based on tetraphenylethene for high-performance CO2 capture and supercapacitor. *Molecules* **26**, 738 (2021).
78. Abdelnaby, M. M. *et al.* Azo-linked porous organic polymers for selective carbon dioxide capture and metal ion removal. *ACS Omega* **7**, 14535–14543 (2022).
79. Abid, A., Razzaque, S., Hussain, I. & Tan, B. J. M. Eco-friendly phosphorus and nitrogen-rich inorganic-organic hybrid hypercrosslinked porous polymers via a low-cost strategy. *Macromolecules* **54**, 5848–5855 (2021).

Acknowledgements

Author contributions

Conceptualization, A.A. and B.T.; methodology, A.A, S.R., and I.A.; software, R.I. and S.N; validation, WAA,; formal analysis, A.K.Q.; investigation, S.R.; resources, A.A, M.R, WAA; data curation, S.A. and S.N.; writing original draft preparation, A.K.Q, I.A and S.R; writing—review and editing, M.R.; A.A.; A.K.Q; . Visualization, R.I, S.A; supervision, A.A.; project administration, B.T.

Funding

Competing interests

The authors declare no competing interests.

Additional information

Correspondence and requests for materials should be addressed to A.K.Q. or M.R.

Reprints and permissions information is available at www.nature.com/reprints.

Publisher's note Springer Nature remains neutral with regard to jurisdictional claims in published maps and institutional affiliations.